2008

RFCCD Microthruster Performance via Numerical Simulation

William B. Stein
Purdue University

Alina A. Alexeenko
Purdue University - Main Campus, alexeenk@purdue.edu

Ivana Hrbud
Purdue University

46th AIAA Aerospace Sciences Meeting and Exhibit
7 - 10 January 2008, Reno, Nevada

AIAA 2008-962

RFCCD Microthruster Performance via Numerical Simulation

William B. Stein*, Alina A. Alexeenko†, and Ivana Hrbud‡
Purdue University, West Lafayette, IN 49707, U.S.A.

Particle-in-cell/Monte Carlo (PIC/MCC) and Direct Simulation Monte Carlo (DSMC) algorithms comprise a numerical model to assess the propulsive capability of a RF plasma microthruster concept. This thruster concept is an electrothermal device and exploits RF capacitively coupled discharge (RFCCD) to heat a propellant. This RF plasma microthruster has potential to alleviate some severe constraints on microsatellite propulsion systems such as power, mass, volume and lifetime. The discharge characteristics are investigated by permuting electrode geometry (0.5 - 10 mm) and applied voltage (10 - 500 V) at a constant RF frequency of 200 MHz and a pressure of 3 Torr. PIC/MCC simulations determine the overall trends in plasma characteristics within this parameter space. The PIC/MCC modeling showed that increases in applied potential and inner radius transmit more power to the fluid. A gas heat transfer model enhanced the original PIC/MCC code to reflect effects of neutral gas temperature in the plasma.

Nomenclature

α_v	Viscosity-Temperature Exponent	
$\bar{T}_{ng}$	Volume Averaged Neutral Temperature	K
Δt	Time-step	s
ϵ_e	Electron Energy	eV
ϵ_i	Ion Energy	eV
η_{PC}	Ratio of Power Loss to Fluid to Total Power Loss	
λ_{DE}	Debye Length	m
ν_m	Electron-Neutral Collision Frequency	MHz
ω_f	Angular Applied RF Frequency	s^{-1}
ω_p	Plasma Frequency	s^{-1}
ϕ	Applied Potential	V
σ_{cx}	Ionization Cross-Section	m^2
σ_{el_e}	Elastic Cross-Section, Electron	m^2
σ_{el_i}	Elastic Cross-Section, Ion	m^2
σ_{ex}	Excitation Cross-Section	m^2
σ_{iz}	Ionization Cross-Section	m^2
$\vec{E}$	Electric Field	Vm^{-1}
d_{gap}	Gap Length of Discharge	m
E/n	Reduced Electric Field	$V \cdot m^2$
E_{ex}	Excitation Energy	eV
E_{iz}	Ionization Energy	eV
f	Applied RF Frequency	Hz
IR	Inner Radius	mm
j	Current Density	Am^{-2}
k	Thermal Conductivity	$Wm^{-1}K^{-1}$

*Ph.D. Candidate, E-mail: steinw@purdue.edu, AIAA Student Member.
†Assistant Professor, E-mail: alexeenk@purdue.edu, AIAA Member
‡Assistant Professor, E-mail: ihrbud@purdue.edu, AIAA Member

n	Neutral Gas Number Density	m^{-3}
n_e	Electron Number Density	m^{-3}
n_i	Ion Number Density	m^{-3}
nc	Number of Computational Cells	
$nc2p$	Ratio of Physical Particles to Computational Particles	
P	Pressure	$Torr$
P_{ref}	Reference Pressure (1 Torr)	$Torr$
PLC	Power Loss to Collisions	W
PLC_{cx}	Power Loss to Charge Exchange Collisions	W
PLC_{el}	Power Loss to Elastic Collisions	W
PLC_{ex}	Power Loss to Excitation Collisions	W
PLC_i	Power Loss to Ionization Collisions	W
PLF	Power Loss to Fluid	W
PLW	Power Loss to Walls	W
T	Temperature	K
T_{ref}	Reference Temperature (300 K)	K

I. Motivation and Background

Since mid-90s microsatellites (mass less than 100 kg) have been identified as enabling concept for various future industry, military and science space missions. Microsatellites offer considerable value and effectiveness over a wide range of applications. Low complexity, manageable development, availability and applicability of low-cost technologies, low mass, low launch costs and non-conventional launch alternatives (piggy-back options) are attractive factors for many application needs. Besides the traditional demands by industry, academia, government and military agencies, developing countries around the world have deployed and are considering microsatellites as significant tools for disaster warning and farming among others due to their attractive attributes. To date close to 100 small satellites (s/c mass below 250 kg) have been launched into orbit. Notably, there has been a fast growth in the number of nanosatellite (mass of 20 kg and less) launched per year in the last decade.[1] These spacecraft are launched into orbits above 400 km with various inclinations to fulfill the specific need of the mission objective. The majority of these satellites possess no propulsion capability, while some are equipped with thrusters for initial orbit insertion such as cold gas microthrusters (SNAP-1),[2] chemical thrusters (XSS-10), micro pulsed plasma thrusters (FalconSat-3),[3] and Hall thrusters (TacSat-2).[4] An example of industrial microsattelite program is ORBCOMM, one of very few fully deployed microsatellite constellation platforms that have 29 satellites in LEO, each equipped with a cold gas thruster for initial orbit insertion, but without any fuel allocation for stationkeeping.[5] With the upcoming launch of the LISA Pathfinder Mission in 2009, micro-Newton colloidal thrusters will be tested on orbit as a part of the disturbance reduction system (ST7-DRS).[6] ST7-DRS is a technology demonstration mission sponsored by NASA New Millennium Program, which initiated research and development of advanced technologies for spacecraft. One of its major aspects is miniaturization to support high launch frequency of small, low-cost spacecraft. To date, this program spun off many micropropulsion system developments of both chemical and electric propulsion technologies. A prospective micropropulsion concept relies on a capacitive RF discharge between co-axial electrodes. The present paper explores numerical methods to assess propulsive capabilities of this concept as a potential micropropulsion system.

A Radio-Frequency Capacitively Coupled Discharge(RFCCD) is a type of gas discharge created by oscillating an applied potential across two electrodes at RF frequencies. The RFCCD is time variant, operates using both displacement and conduction currents and consists of two major regions. The discharge is composed of a central quasi-neutral region which is analogous to the positive column of a DC glow discharge and sheath regions which exist between the quasi-neutral core and each electrode. The sizes of each region depend on the operating pressure, applied voltage, and electrode sizes.[7] The creation of sheaths represents a change in electron/ion number density due to electron/ion diffusion into the electrode itself and whose structure oscillates with the applied field. The energy of the applied electric field in RF discharge is being transferred to the bulk gas due to collisions between plasma species and the neutral propellant. The resulting plasma heating of the propellant can be exploited for electrothermal propulsion.

While this thruster technology is relatively new, RF discharges have been previously utilized as a propulsion mechanism, albeit in different ways.[8–14] RF has been used as either a means for ion production in

electrostatic thrusters, or a means to heat a fluid similarly to a microwave thruster operating a much lower frequency. RFCCD utilizes the RF component to contain as well as heat the ions produced by the glow discharge. The RFCCD has been investigated most extensively in the application to etching and sputtering.[15,16] Etching/sputtering research is primarily devoted to a low-pressure discharge in argon with a goal to effectively sputter or etch the target material and not necessarily with a goal of heating the fluid. While the process is effectively the same, the objectives of a sputtering/etching discharge is the opposite of those required for an RF plasma thruster operation. Work has also been done regarding the use of different gases within the discharge.[17–22] These investigations illustrate differences and possible benefits of utilizing different propellants for the RFCCD microthruster.

The most technically similar work was performed in 1999[23,24] and focused primarily on investigating electrode erosion and the effect of characteristic operating parameters such as massflow, applied frequency, applied power, and electrode separation distance. It was performed with a large "proof-of-concept" thruster having an inner electrode diameter of approximately 5 cm. This work illustrated a reduction in electrode erosion when compared to operation in a DC mode as well as a small rise in temperature within the thruster.

Our previous work[25] investigated the effects of pressure and frequency on performance of a 50W RFCCD microthruster. This was done at a constant applied potential and inner radius corresponding to conditions similar to that in the experiments.[26] One selected favorable discharge case (3 Torr, 500 V, 200 MHz) and the corresponding plasma densities and gas heating formed the basis for an in-depth flow field and thrust performance analysis using the DSMC method. Assuming adiabatic wall conditions, the RF plasma thruster achieved a specific impulse of 104.4 s with argon at a throat Reynolds number of about 25. The RF heating increases the specific impulse by 125 % compared to cold gas thruster at the same geometry and pressure. The present work focuses on studying the effect of varying the discharge chamber radius and voltage on the plasma properties. This study also discusses the integration of a gas heat transfer model within the PIC/MCC method for self-consistent plasma simulations and the effects this has on the microthruster performance.

II. Experimental Assessment of the RF Plasma Microthruster Concept

The RFCCD microthruster is based on RF capacitively coupled discharge between coaxial electrodes. Figure 1 illustrates the basic geometry and configuration underlying this proposed propulsion system. The basic idea of this concept lent itself to the supposition that electrode wear (sputtering, erosion) could be significantly reduced or even eliminated with geometry and electrical characteristics. Preliminary proof-of-concept experiments were conducted at Auburn University.[23,27] The main goal of that study was to explore feasibility of the concept regarding possible propulsive capability for small satellite applications. Furthermore, it evaluated fundamental operating characteristics as a function of frequency, power, and mass flow rate. Under certain operating characteristics electrode wear was suppressed.

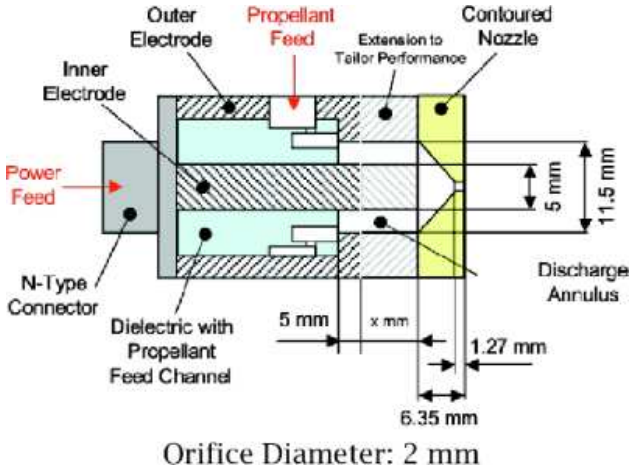

(a) Schematic of the RF Plasma Microthruster Concept

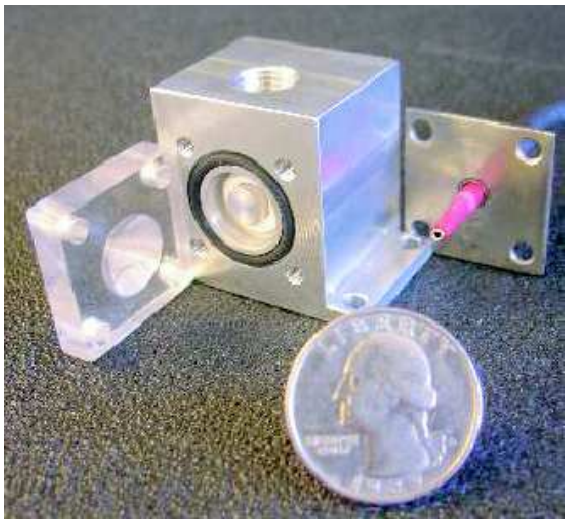

(b) Hardware of Test Article RF25-1

Figure 1. Schematic and Hardware of RF microthruster

This RF plasma concept is classified as an electrothermal system. RF power is fed co-axially to the inner and outer electrodes. Similarly, propellant is injected into the cavity formed by the electrodes. Two second-generation test articles, designated RF25-1 and RF50-1, were designed and built using the same principle coaxial layout. Figure 1 shows a schematic of the basic design and indicates typical dimensions of the smaller test article. The inner electrode diameters are 0.64 cm and 1.27 cm, respectively. The RF powertrain, consisting of a HP frequency generator, a RF power amplifier, RF power meter, transmission lines and vacuum feedthroughs, is based on 50-Ω transmission lines. Based on coaxial transmission line theory, the inner/outer electrode geometry maintains a 50-Ω impedance, minimizing impedance mismatch and power loss across the thruster. The dielectric spacer is made of machineable alumina bisque. It provides electrode separation and incorporates an elegant solution to introduce the propellant into the discharge annulus. It features radial propellant feed and axial propellant injection into the annulus between the electrodes. Electrodes are made of aluminum while a contoured nozzle is machined from Lexan. The two laboratory-scale test articles have a mass of 113 g and 229 g, respectively. Both are compact cubes, where the sides of the cube measure about 3.8 cm for RF25-1 (55 cm3) and 4.5 cm for RF50-1 (85 cm3). Neither of the two laboratory test articles represents a mass or volume optimized design. Preliminary experiments were conducted with both test articles under various test conditions to explore operating regimes. Helium, nitrogen, and argon served as propellants. DC and RF power supplies provided a range of different electrical conditions at power levels below 100 W. The main objective of these experiments was to understand the control and its resulting behavior of a significantly smaller RF plasma thruster.[26] A vital parameter controlling propulsive capability of electrothermal devices is the amount of power coupled into the plasma. To access this particular characteristic, experiments were conducted to determine the influence of heating on the pressure in the discharge annulus. The pressure in the discharge annulus is established in two ways. Propellant was fed using a 50-sccm mass flow controller or directly from the pressurized gas bottle using a regulator. A cold-gas baseline was established by measuring the pressure in the discharge annulus as a function of mass flow rate and orifice diameter. This baseline is then compared to the pressure with RF heating at various frequencies. Figure 2(a) and 2(b) show the pressure in the discharge annulus as a function of mass flow rate, power input and frequency. This data reflects the behavior of the RF25-1 with an orifice diameter of 0.711 mm using nitrogen or argon as propellant. RF heating increases the enthalpy of the propellant. Pressure is a function of both power and mass flow rate.

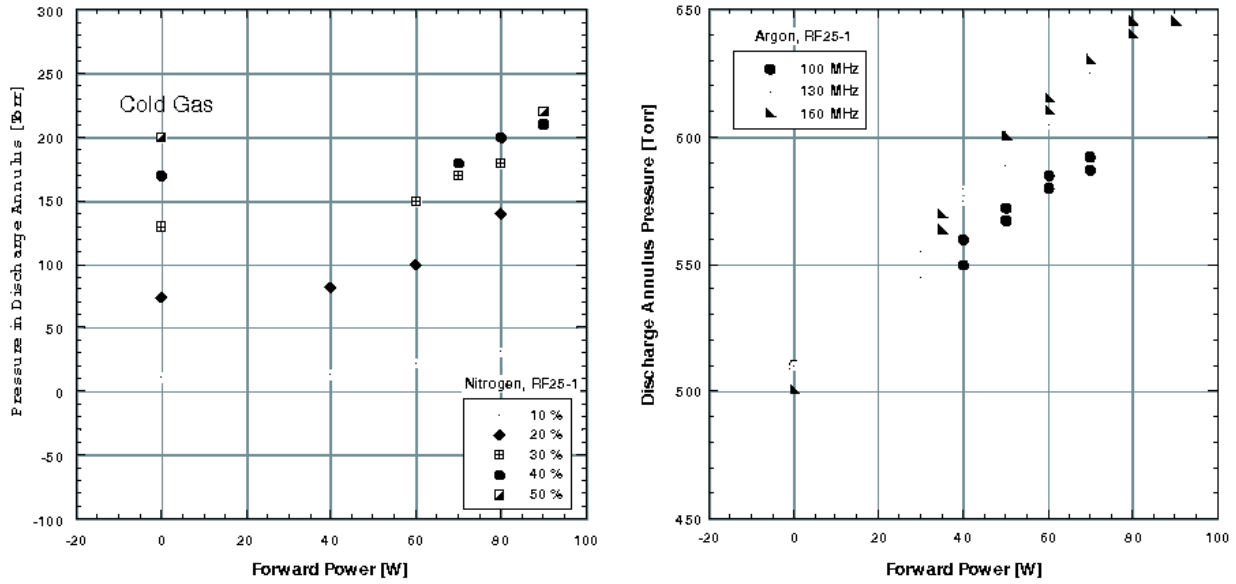

(a) Pressure as a Function of Power and Mass Flow Rate for Nitrogen at 160 MHz

(b) Pressure as a Function of Power and Frequency for Argon

Figure 2. Pressure Measurements as a Function of Power, Mass Flow Rate and RF Frequency.

III. Modeling Approach

A. PIC/MCC Modeling

The modeling approach combined both PIC and DSMC methods for performance analysis of RF plasma thruster. To address the nature of small satellite applications the control parameters encompass pressure, electrode size, frequency and power input. This investigation considers electric power delivered at frequencies of 200 MHz and voltages between 10 and 500 V. The pressure in the discharge chamber being 3 Torr. The geometric design of the thruster corresponds to prototypes studied experimentally at Purdue. The thruster discharge chamber is bounded by coaxial electrodes that is attached to a converging Lexan nozzle with a 2 mm diameter orifice. The PIC plasma simulations are applied for the discharge chamber with a successive DSMC simulations of the propellant expansion through the orifice into vacuum conditions.

The Particle-In-Cell/Monte Carlo Collision (PIC/MCC)[28] method is currently the most powerful approach for kinetic plasma modeling in the collisional regime is used to determine plasma characteristics within the coaxial discharge chamber. The charged test particles in PIC/MCC method move in the electric field and representative collisions between charged and neutral particles are calculated using Monte Carlo method. Our model utilizes *XPDC1*, a one dimensional, bounded, cylindrical plasma simulation code developed by the Plasma Theory and Simulation Group at the University of California at Berkeley. Argon collisional model employed in *XPDC1* includes electron-neutral ionization, lumped excitation and elastic scattering using Lawler-Kortsghagen cross-sections.[29] The ion-neutral charge exchange and elastic scattering are also incorporated.[30] The computational parameters of PIC model were chosen to meet the criteria specified below for numerical accuracy:

- Number of Cells: $nc \geq \frac{2d_{gap}}{\lambda_{DE}}$
- Time-step: $\Delta t \leq \frac{0.2}{\omega_p}$ -and- $\Delta t \leq \frac{1}{\omega_f}$
- Ratio of Physical Particles to Computational Particles: $nc2p \approx$ 50-100 computational particles per cell at steady state

B. Gas Heat Transfer (GHT) Modeling

The original code *xpdc1*, was augmented to incorporate changes in gas heat transfer as a result of plasma heating. Since the main goal of these simulations is to study the performance and behavior of a microthruster which utilizes an RFCCD to heat a working fluid, the effects of heating the working fluid should be included in the plasma simulation. The main function of *xpdc1* is to model different plasma discharges at lower, more rarefied pressures where modeling via PIC simulations is efficient. Within this realm heat transfer to the neutral gas species can be considered negligible and thus not regarded. The investigation of RFCCD microthruster performance borders on the periphery of this modeling regime and must range from a collisionless regime to that of continuity. Changes in gas temperature become more prevalent as the fluid becomes continuum. Thus, gas temperature variation must be incorporated in order to make the simulation self-consistent within sub-continuum and continuum regimes of microthruster application. These modifications were performed using a two step process; vectorization of the appropriate variables and the integration of a temperature solver.

The gas temperature in the original code was set to a constant scalar value throughout each simulation. In order to properly solve for a temperature distribution throughout the discharge, the neutral gas temperature was vectorized such that it can be calculated in each cell. This modification resulted in the vectorization of many other variables which are dependent on the neutral gas temperature. This also provides the ability to create distributions of the gas density, different collision frequencies, and power losses due the different collision mechanisms.

The gas temperature is then calculated based on period-averaged power loss to the fluid by solving the heat conduction equation in the coaxial electrode gap with fixed temperature boundary conditions. This is traditionally solved using joule heating[31] in diffusion-drift plasma approximation. In PIC simulations, it is possible to utilize the actual power transmission that occurs in various types of plasma-neutral collisions. This aims to incorporate both joule and stochastic heating on a particle-by-particle level.

$$-\frac{1}{r}\frac{\partial}{\partial r}\left[rk\frac{\partial T}{\partial r}\right] =< PLF > \tag{1}$$

Here T is the gas temperature, k is the thermal conductivity, and the angle brackets on the right-hand side denote period-averaged quantities. Four power loss factors are calculated in this simulation, power lost to elastic, charge exchange collisions, ionization, and power lost to excitation collisions; PLC_{el}, PLC_{cx}, PLC_i, PLC_{ex}. The power lost to the fluid, PLF , consists of the first two power loss mechanisms. Electrons can collide with neutrals either elastically, via ionization or excitation collisions whereas ion-neutral collisions may either be elastic or charge-exchange in nature. Elastic and charge-exchange collisions directly transfer energy between the plasma and the neutrals. Conversely, ionization collisions create ion-electron pairs which help sustain the plasma and offset both recombination and diffusion losses. The energy remaining after the ionization event is directly transferred to the new ion/electron pair, not the neutrals. The power lost to excitation collisions is regarded as a similar loss mechanism to ionization and is not used to heat the working fluid. PLC_{ex} is lost via the excitation of electrons within the outer valence shells of the neutral molecules. This energy is then reemitted via a "glow". While it is understood that some of the photonic power reemitted from the excited neutrals can be used to heat the fluid, it is believed to be small in comparison to the sum of the other heating mechanisms. Currently no model is utilized within the PIC simulation to calculate power transmitted via photonic emission.

The neutral gas temperature is calculated using Gaussian elimination with partial pivoting every 1000 time steps. Time averages over this time-frame for the power lost to the fluid are used to solve for the temperature distribution throughout the discharge. The temperature-dependent thermal conductivity of the neutral gas:

$$k = k_{ref} \left(\frac{T}{T_{ref}} \right)^{\omega} \tag{2}$$

is found using the previous temperature distribution. Here $k_{ref} = 0.01637$ W m^{-1} K^{-1} and T_{ref}=300 K. The temperature boundary conditions for this investigation have been set to 300 K which is typical for the initial stage of thruster operation. The wall thermal boundary conditions are more dependent on a specific thruster design and implementation than the discharge itself. More detailed boundary conditions can be applied in a full coupled solid-fluid heat transfer model which is beyond the scope of this investigation. The results of these modifications have been verified by comparison with analytical heat transfer solutions and the original PIC/MCC constant-temperature solutions but have yet to be experimentally validated.

C. DSMC Modeling

The direct simulation Monte Carlo (DSMC) method is applied to model the neutral gas expansion in the region from the RF discharge annulus to the vacuum chamber. A kinetic approach to modeling neutral gas flow in the thruster is needed due to significant effects of rarefaction in the operating pressure range (mTorr - Torr). The value of the Knudsen number based on the orifice radius of 1 mm is about 0.04 at p=1 Torr and $T = 300$ K. The axisymmetric DSMC code SMILE[32] is applied with variable-hard-sphere model, molecular diameter of $d = 4.17 \times 10^{-10}$ m and the viscosity-temperature exponent $\alpha_v = 0.31$ for argon. Finally, the RF thruster performance parameters such as thrust, mass flow rate and specific impulse are calculated based on the DSMC solution at the orifice exit plane and compared with that for cold gas expansion for the same geometry and pressure.

IV. Results and Discussion

A. Inner Radius Versus Applied Potential (IRvV)

One of the main goals of this investigation is to observe effects regarding changes in inner radius versus applied potential. Changes in these two parameters dictate variations in the reduced electric field, and hence the structure of the discharge itself. For this investigation the outer electrode radius, and thus the thruster geometry, is defined such that the thruster impedance (in vacuo) is approximately 50 Ω. Thus, varying the inner electrode alone scales the interelectrode gap, and consequently the discharge volume. It is understood that these two parameters do not solely dictate the discharge characteristics but for scope of this investigation these two parameters are varied at a constant pressure and applied frequency.

Investigating variation of the inner radius and applied potential produces information regarding thruster scalability and the applicability of using satellite bus voltages directly without any need for voltage condi-

tioning. It is believed that there are effective limits on both the inner radius (i.e. interelectrode gap distance) and the applied potential corresponding to limits of the discharge physics. The applied potential and inner radius must be in a configuration for which a discharge can not only be initiated at these conditions, but also sustained. Thus, a balance between ionization and electron diffusion/recombination must be achieved to create and sustain a plasma discharge. If the ionization rate is too low (as with too small a electron temperature) or the diffusion rates are too high (with high surface area to volume ratios) a discharge will not be sustained. Also, for larger inner radii/larger volumes, too much power will be absorbed by the plasma which may exceed the power availability constrained by the satellite. At higher reduced electric fields, the physical characteristics of the discharge change; shifting the discharge from an α type to that of a γ type or even possibly that of an glow-arc transition.

The limits of these parameters range from 0.5 mm to 1 cm for the inner radius and 10 V to 500 V for the applied potential. The ranges of these variables were determined from both previous studies[25] and the desire to investigate the lower operating limits for both the applied potential and thruster size. The power lost to the fluid and the power transmission efficiency for this study are shown in Figure 3.

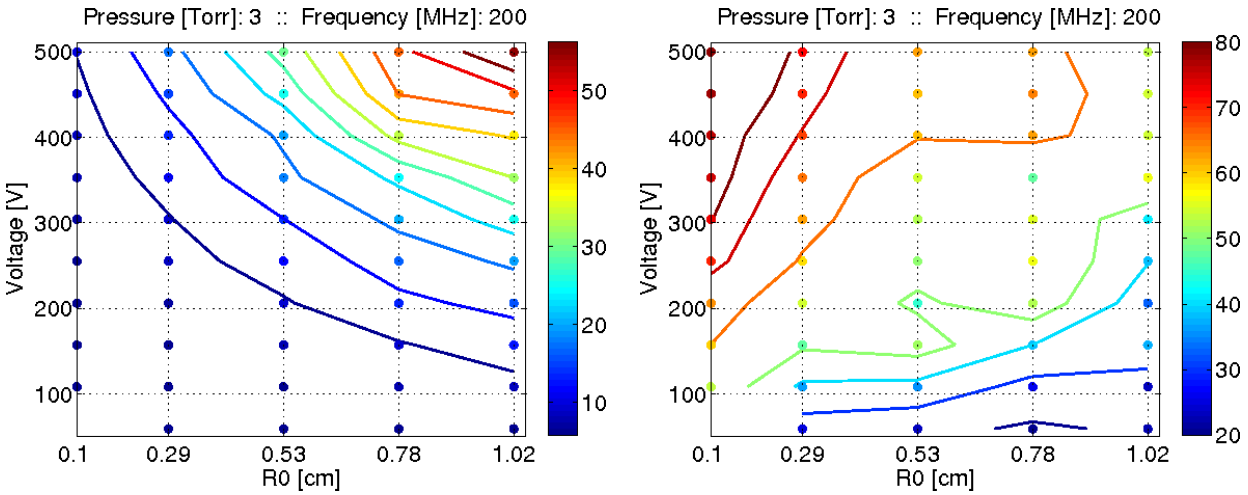

(a) Power Lost to Fluid (W)

(b) η_{PC}

Figure 3. IRvV Results

One can see power lost to the fluid increases with an increase in potential or an increase in inner radius. Since the power lost to the fluid is mainly comprised of the power lost to charge exchange collisions, any trends shown in PLF can be explained via trends in PLC_{cx}. Increasing the applied potential increases the potential drop through each sheath. This increase causes the ions to accelerate faster within the sheath, thus increasing the power transmission of each ion-neutral collision. An increase in inner radius increases the volume of the discharge. This translates into a higher collision rate within the discharge at a constant number density, and thus correspondingly increases the amount of power transmitted to the fluid.

This study also found lower limits to both the inner radius and potential. Discharges simulated at 10 V exhibited very little ionization and not enough to sustain the discharge. Also, discharges simulated with an inner radius of 0.5 mm could not be sustained regardless of potential. Mainly, the electron diffusion/recombination rates were too high (especially at higher voltages) to fully sustain the discharge.

In terms of the power transmission efficiency, higher voltages and lower inner radii are preferred. Increasing the either applied potential or the inner radius not only increases the power transmitted via charge exchange collisions, but the power lost to both ionization and excitation collisions as well as power lost to the walls. Over the range of this study, PLC_{cx} and PLC_{ex} both range from about 5-25 W and PLC_i ranges from about 5-6 W. Thus, the majority of the power transmission inefficiency comes from the excitation component.

The power lost to excitation collisions and power lost to the wall must be minimized in order to make power transmission to the fluid more efficient. Power lost to ionization is required to sustain the discharge eventhough it does not directly heat the neutral gas. A means to achieve more efficient power transmission can be illustrated by comparing the various cross-sections utilized in this simulation. The Lawler-Kortsghagen cross-section[29] relations and the ion-neutral cross-section[30] relations given as Equations 3-8

$$\sigma_{iz} = 3.18 \times 10^{-20} \frac{\ln \frac{\epsilon_e}{E_{iz}}}{\frac{\epsilon_e}{E_{iz}}} \qquad \frac{\epsilon_e}{E_{iz}} > 1 \tag{3}$$

$$\sigma_{ex} = 1.56 \times 10^{-20} \frac{\ln \frac{\epsilon_e}{E_{ex}}}{\frac{\epsilon_e}{E_{ex}}} \qquad \frac{\epsilon_e}{E_{ex}} > 1 \tag{4}$$

$$\sigma_{el_e} = 1.59 \times 10^{-19} \frac{\epsilon_e}{11.55} \qquad \epsilon \leq 11.55eV \tag{5}$$

$$\sigma_{el_e} = 1.59 \times 10^{-19} \sqrt{\frac{\epsilon_e}{11.55}} \qquad \epsilon > 11.55eV \tag{6}$$

$$\sigma_{el_i} = (7.0 \ - 0.380 \ln \epsilon_i)^2 \times 10^{-20} \tag{7}$$

$$\sigma_{cx} = (6.45 - 0.365 \ln \epsilon_i)^2 \times 10^{-20} \tag{8}$$

where $E_{iz} = 15.76$eV and $E_{ex} = 11.62$ eV for argon. Notice that the cross-section relations for ionization and excitation have a similar form. Figure 4 (a) illustrates the excitation and ionization cross-sections as a function of electron temperature.

By comparing both cross-sections, it can be shown that the excitation cross-section can be minimized with an increase in electron temperature, but approaches a minimum of approximately 42% relative to the ionization cross-sections. Unfortunately, the excitation cross-section for an RFCCD discharge will always be larger than the ionization cross-sections since typical electron temperatures are less than 10 eV. Thus, power loss to excitation will always be present but can be minimized by increasing the electron temperature. In terms of power loss mechanisms, this can be reduced by increasing the voltage and decreasing the inner radius and is shown in Figure 4 (b). Comparing this with the power lost via charge exchange shows that while both the excitation and charge exchange mechanisms increase with both voltage and inner radius, the charge exchange power loss increases faster than that due to excitation for increasing voltage. This is due to the fact that the ion temperature increases at a faster rate than the electron temperature for an increase in potential and can also explain the η_{pc} trends shown in Figure 3(b). Figure 5 compares distributions of

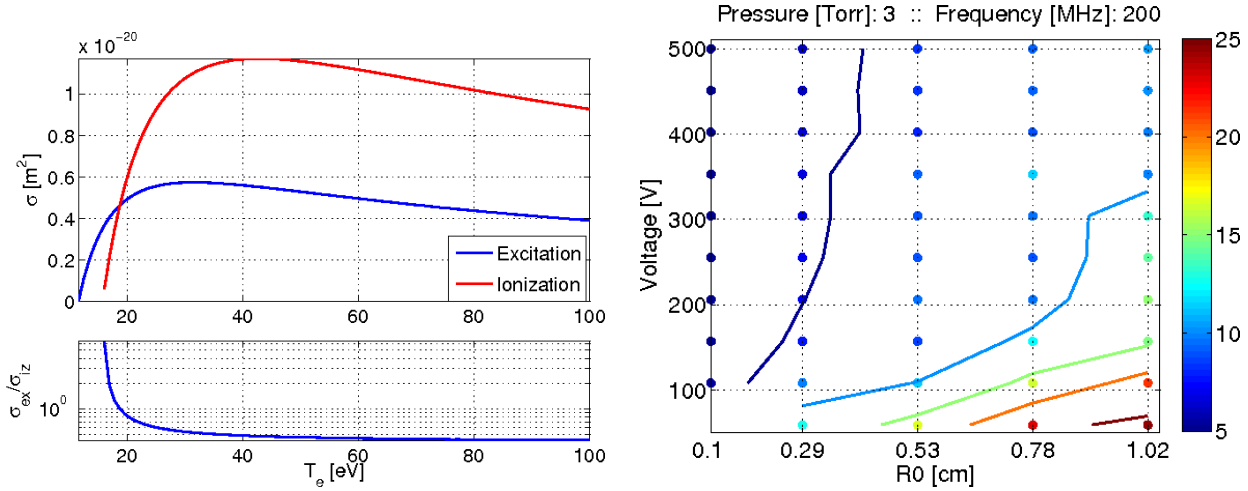

(a) Ionization and Excitation Cross-Sections (b) Power Lost to Excitation/Ionization

Figure 4. Cross-Section Results

the various power loss mechanisms for two cases using gas heat transfer (see Section B). It can be shown in both cases that charge exchange power loss is the largest component of PLF. The elastic power losses tend to be negligible when compared to the other three power loss mechanisms. Elastic electron-neutral collisions, while the most probable collision, tend to transfer very little energy to the neutral gas due to the electrons small size. Elastic ion-neutral collisions transfer a small amount of energy as well due to their lower velocities in the quasi-neutral region. Only in the sheath regions where the potential drop is larger does an ion attain enough velocity to exhibit useful energy transfer; being where charge exchange collisions mainly

take place. An increase in potential increases the magnitude of the potential drops across both sheaths and causes the ions to accelerate faster through the sheath region, thus providing more power loss via charge exchange collisions. Elastic collisions are affected differently by potential increases. An increase in potential has little effect on elastic ion-neutral collisions since the majority of the potential is applied to the sheaths and not the quasi-neutral region. An increase in potential transitions elastic electron-neutral collisions to either an excitation collision or even possibly an ionization collision given a high enough potential.

In terms of the other power loss mechanisms, power loss to excitation mainly occurs in the quasi-neutral, central region of the discharge indicative of an α type RFCCD. The power loss to excitation contributes to the amount of light emitted by the discharge, and thus defines the "glow" region. Power loss to ionization occurs mainly in the pre-sheath regions and helps create the dual-peak plasma number density distributions. As the voltage is increased both ionization and excitation become more prevalent in the discharge. In terms of ionization, this increase in voltage increases the number of ionization collisions and thus exaggerates the pre-sheath peaks. An increase in voltage also increases the power lost to excitation, thus making the discharge "glow" brighter.

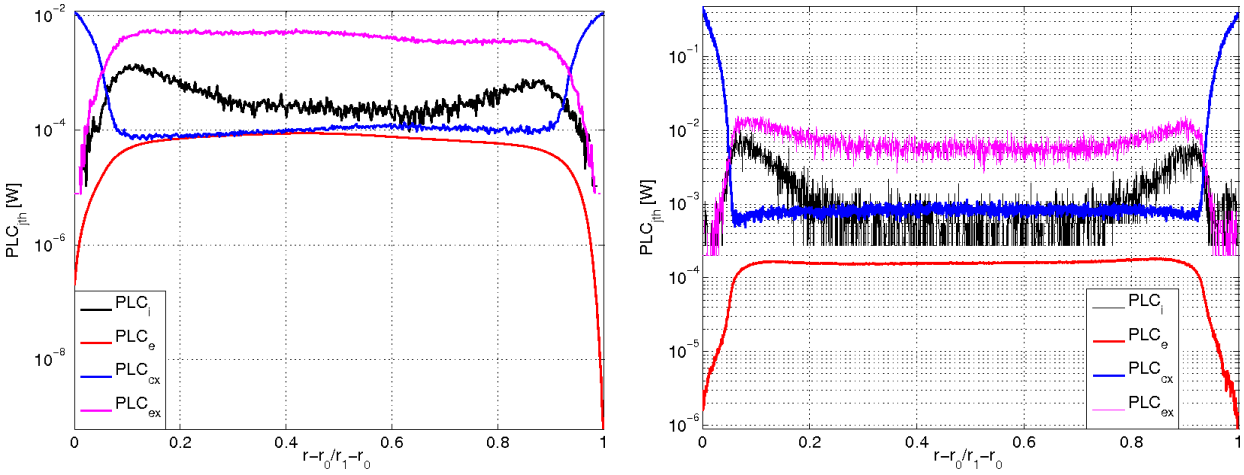

(a) 3 mm, 59 V (b) 5 mm, 500 V

Figure 5. Power Loss Mechanisms

Individual electron number density distributions were also compared as a function of either inner radius or applied voltage. These comparisons are shown in Figure 6 which illustrates electron number density as a function of a non-dimensional radius[a].

It can be shown that increasing the applied potential at a constant radius not only increases the magnitude of the electron number density, but also alters its shape. At lower potentials, the electron number density has a flatter distribution than those at higher potentials. As the potential is increased, the sheath near the live electrode becomes sharper and more prominent, but also contains more electrons within the sheath itself. A similar effect is shown in the grounded sheath. A potential also exists beyond which the distribution transitions from a flat distribution into one with exacerbated pre-sheaths. Further increase in potential increases the overall number density, but also tends to make the pre-sheath number densities more pronounced.

It can also be shown that an increase in inner radius, and hence discharge volume, at a constant potential has no appreciable effect on the magnitude of the electron number density, but increasing the inner radius transitions the discharge in a similar fashion to that of increasing voltage. As the inner radius is increased, the distribution progresses from a flat, uniform discharge to one where the pre-sheath peaks are exacerbated. This effect is similar in nature to an increase in voltage without an increase in overall electron number density. Since the overall number density is roughly constant, there is an increase in the overall number of collisions within the larger discharge volume. Thus, increasing the inner radius increases the ionization rate in the pre-sheath thus transitioning the discharge from a flatter distribution to one with two pre-sheath peaks.

[a]0 corresponds to the inner electrode and unity corresponds to the outer electrode

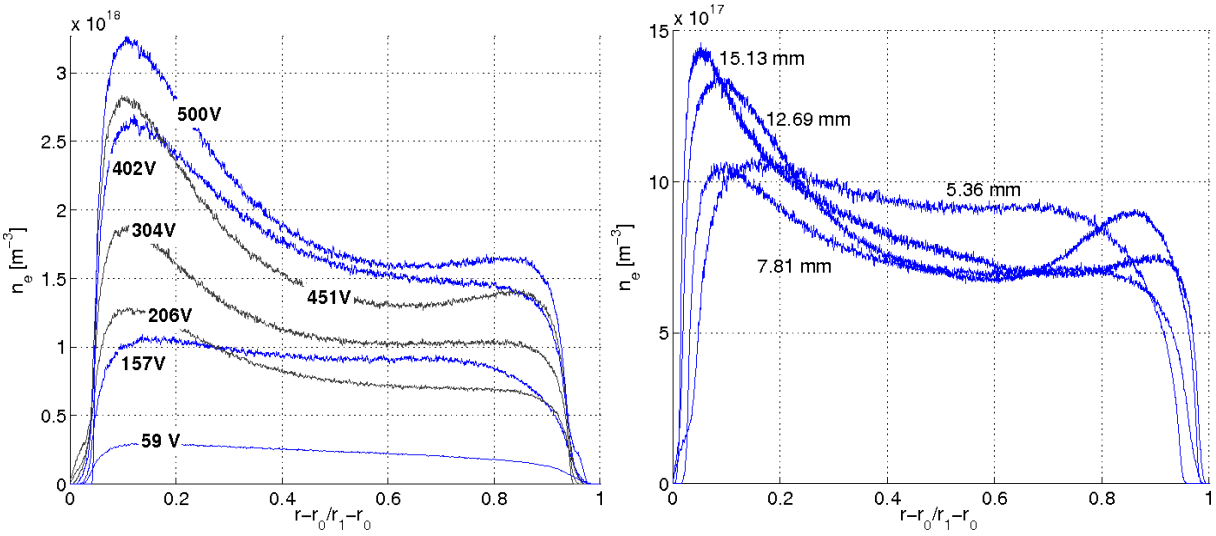

(a) Voltage Variation: IR: 5.38 mm (b) Inner Radius Variation: V: 157 V

Figure 6. Comparison of Electron Number Density Profiles

B. Gas Heat Transfer Results

The second goal of this investigation is to better understand how gas heat transfer affects the characteristics of a plasma discharge as well as performance implications of an RFCCD microthruster. Three cases were analyzed corresponding to a lower and higher power both with and without gas heat transfer. The results from this analysis are shown in Table 1.

Table 1. Comparison of Data with and without Variable Neutral Gas Temperature Method

Case	$\bar{T}_{ng}$ [K]	n_0 $[m^{-3}]$	PLF [W]	PLC_{ex}	PLC_{iz} [W]	PLW [W]	η_{PC}
3 Torr, 200 MHz, 3 mm, 59 V							
Constant Gas Temperature	300.00	1.57e17	0.30	0.87	0.08	0.009	0.25
GHT with variable k	312.42	1.35e17	0.33	0.66	0.15	0.039	0.17
3 Torr, 200 MHz, 5 mm, 500 V							
Constant Gas Temperature	300.00	1.76e18	32.53	14.01	2.29	0.89	0.69
GHT with variable k	620.34	1.06e18	31.64	20.40	3.81	3.38	0.57

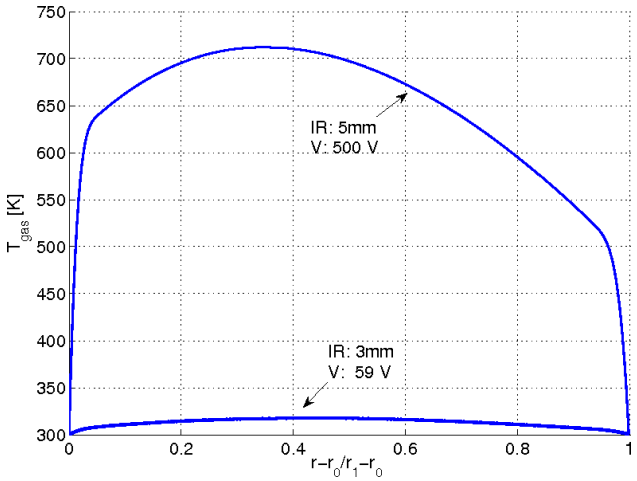

Figure 7. Comparison of Temperature Profiles

The overall effect of neutral gas heat transfer depends on the conditions of thruster operation. Over this range of input conditions (potential and inner radius), the power transmitted into the fluid can vary greatly and changes the effect of neutral gas heat transfer on the discharge. Even with the lower power case, heat transfer to the neutrals is non-negligible. As power is transmitted to the neutral gas, the neutral temperature rises, reducing the gas density and thus the neutral collision frequency. This reduces the plasma's effectiveness to transmit power to the fluid which reduces the gas temperature etc, until the discharge becomes stable. This dependence effectively reduces the power transmission and thus thruster performance to that relative to that without any heat transfer modeling. Thermal conductivity effects are also non-negligible for higher power/higher temperature discharges. The temperature distributions for these three

cases are compared together in Figure 7.

Gas heat transfer not only affects the bulk parameters of the discharge but also the shape of the discharge as well. Electron number densities are compared for both cases in Figure 8. The presence of higher neutral temperatures in the discharge reduce the number densities of the plasma, as aforementioned, but also the shape of the distribution. The increase in neutral temperature effectively similar to a reduction in pressure eventhough the pressure is held constant. For argon the effective frequency of momentum transfer due to collisions is estimated as:[33]

$$\nu_m = 5.3 \times 10^9 \left(\frac{P}{P_{ref}}\right)\left(\frac{T_{ref}}{T}\right) \tag{9}$$

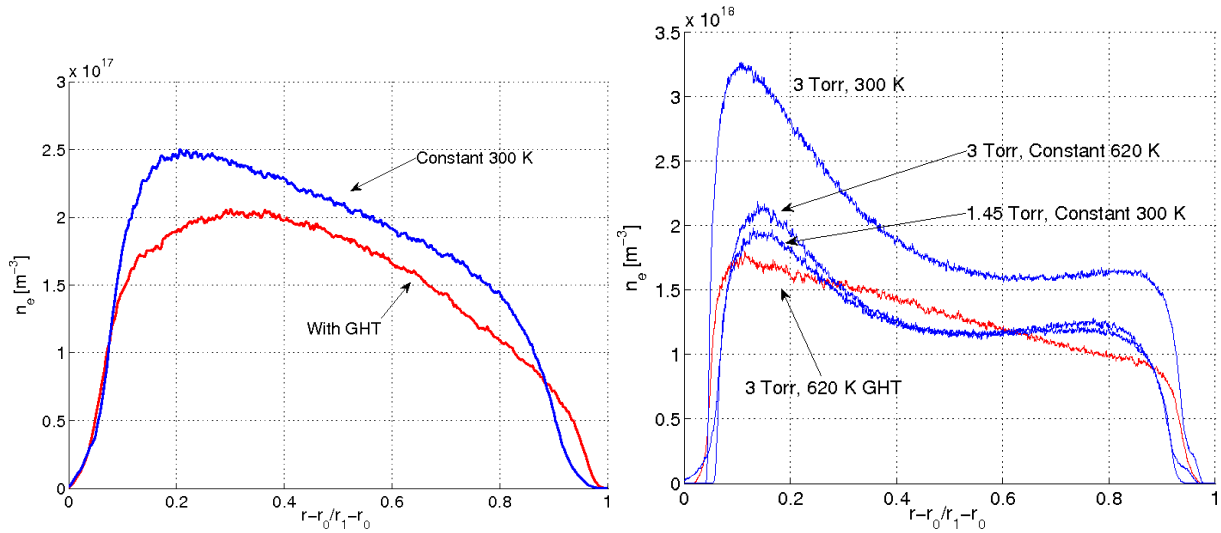

(a) 3 mm, 59 V (b) 5 mm, 500 V

Figure 8. Comparison of Electron Number Density Profiles

Thus, similar discharge characteristics should appear if the pressure is raised with an increase in temperature that attempts to keep the plasma-neutral collisional frequencies constant. This will not exactly be a one-to-one relation given that collision cross-sections, power transmitted to the fluid, and thermal conductivity are all functions of temperature. Also, there will be effects derived from the shape of the temperature distribution itself since it is not constant across the discharge.

Electron number density profiles and bulk parameters of the 5 mm, 500 V case with gas heat transfer are compared to that of a discharge at similar conditions, but with a pressure of 1.45 Torr. This reduction in pressure corresponds to the effective increase in average temperature shown by the addition of gas heat transfer and is shown in Figure 8(b) and Table 2.

Table 2. Comparison of Reduced Effective Pressure on Discharge Parameters

Case	$\bar{T}_{ng}$ [K]	n_0 [m^{-3}]	PLF [W]	PLC_{ex} [W]	PLC_{iz} [W]	PLW [W]	η_{PC}
3 Torr, 200 MHz, 5 mm, 500 V							
Constant Gas Temperature	300.00	1.76e18	32.53	14.01	2.29	0.89	0.69
GHT with variable k	620.34	1.06e18	31.64	20.40	3.81	3.38	0.57
Constant Gas Temperature	620.00	1.10e18	19.60	6.22	1.71	0.38	0.75
1.45 Torr, 200 MHz, 5 mm, 500 V							
Constant Gas Temperature	300.00	1.07e18	19.36	6.53	1.77	0.48	0.73

Figure 8(b) shows the exceptional difference in discharge structure with and without gas heat transfer. The presence of neutral gas heat transfer not only reduces the electron number density as expected with a reduction in plasma-neutral collision frequency, it also reduces both pre-sheath peaks.

Two discharges at 1.45 Torr, 300 K and 3 Torr, 620 K with constant temperature profiles were also compared. These two cases show similar discharge characteristics with the exception of slightly enhanced pre-sheath peaks in the 3 Torr case. This illustrates the fact that plasma-neutral collision frequency influences

the overall number density of the plasma, but the discrepancies indicate that other factors can influence the discharge shape as well. One can also observe the effects of the actual temperature distribution by comparing the 3 Torr, 620 K cases with and without neutral gas heat transfer. The similarity of the trends and distributions exhibited in these three cases reinforce the hypothesis that the plasma-neutral collision frequency is a primary mechanism for creating similar discharges. Secondary mechanisms, like neutral temperature distribution and thermal conductivity, also play a role in determining the discharge characteristics. Equation 9 shows operating at a higher pressure and a lower temperature is beneficial for better power transmission into the fluid, but not necessarily better power generation in general.

Different heat transfer sources were also compared. The current heat transfer model used in this investigation employs the use of PLF as the source term in the conduction equation. This is compared in Figure 9 with the more traditional method of employing joule heating instead.[31]

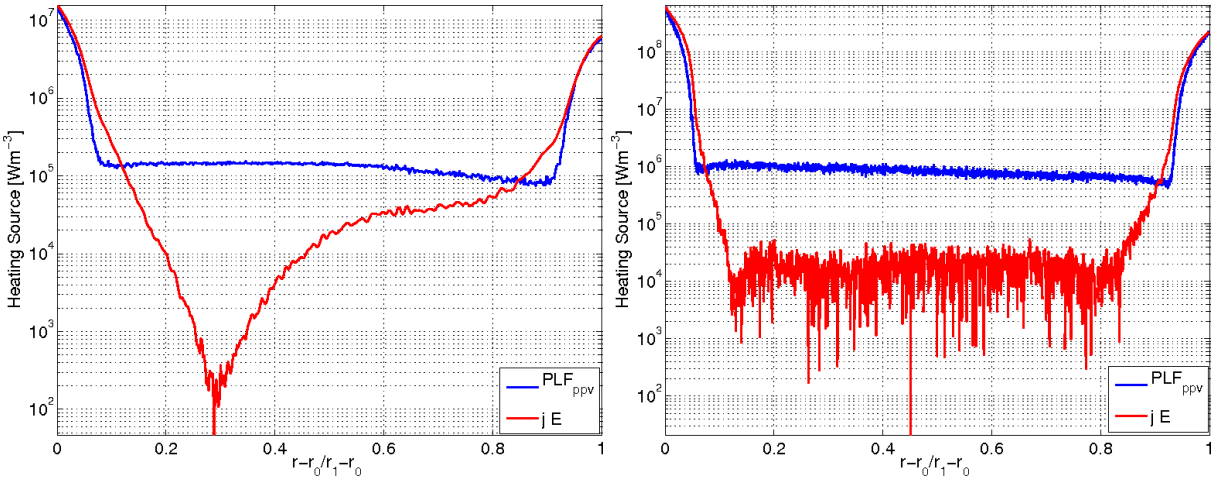

(a) 3 mm, 59 V (b) 5 mm, 500 V

Figure 9. Comparison of Sources Terms in the Heat Conduction Equation

The main difference between these two mechanisms reside in how they are calculated. Joule heating is calculated using $j \cdot E$. Since the potential in the quasi-neutral region is essentially constant, the electric field is correspondingly near zero. This causes $j \cdot E$ to be present primarily in the discharge sheaths and comparatively low in the quasi-neutral region. While this is true, collisions do occur within the quasi-neutral region and power is transmitted, albeit to a lesser extent. Thus utilizing the PLF which is calculated on a particle-by-particle basis is more accurate. This being said, this comparison shows that using joule heating is adequate at larger pressures, since the majority of the heating occurs in the sheaths where the values of PLF and $j \cdot E$ are close.

C. Thruster Performance Comparison

The DSMC modeling was applied to obtain the flowfields and thrust performance of the RF plasma thruster for a pressure of 3 Torr, an applied voltage of 500 V and RF frequency of 200 MHz. The DSMC computational domain is shown in Figure 10 extends from the exit of the discharge chamber and the inner electrode wall at left ($x = 0$) to the converging Lexan-cover nozzle (shown in gray) and the vacuum chamber as the outflow boundary. The inflow boundary at $x = 0$ corresponds to a constant pressure of 3 Torr, zero velocity and a gas temperature variation obtained via PIC/MCC simulations with gas heat transfer. A total of about 4.8 million computational particles and about 0.8 million collision cells were used in the DSMC simulation that took about 24 hours on eight processors of a SunFire 4600.

Table 3. RF thruster performance at a pressure of 3 Torr, applied voltage of 500 V and RF frequency of 200 MHz)

Case	Thrust, mN	Mass flow rate, mg/s	Specific impulse, s
RF Discharge (adiabatic wall)	1.31	1.28	104.4
RF Discharge (adiabatic wall, GHT)	1.38	2.02	69.3
RF Discharge (300 K wall)	1.37	2.25	61.9
Cold gas	1.40	3.08	46.4

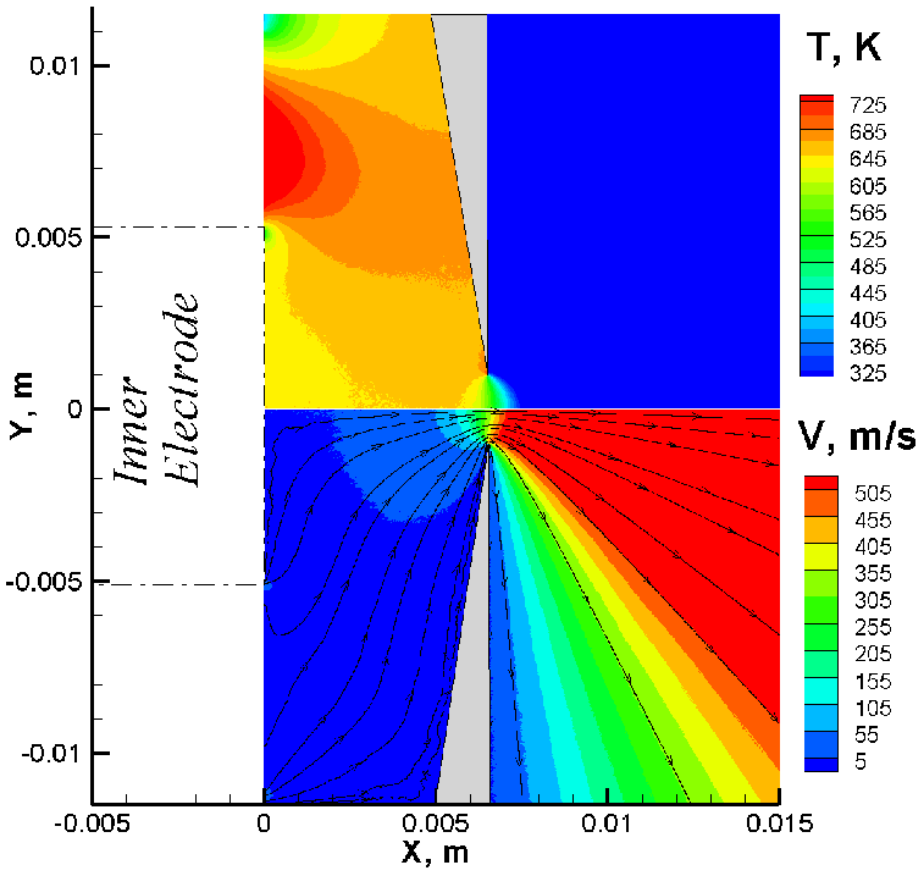

Figure 10. DSMC calculated temperature contours (top) and X-velocity contours and streamlines (bottom).

The calculated thrust, mass flow rate and specific impulse are given in Table 3 for adiabatic and constant wall temperature and with/without gas heat transfer modeling in plasma simulations. Based on this modeling, the gas heat transfer has a significant impact on the predicted specific impulse of the thruster.

V. Conclusions

An RFCCD thruster was modeled using a combination of PIC and DSMC simulations. It has been demonstrated that there is a required minimum applied potential and minimum inner radius such that the discharge can be sustained. Thruster performance can be increased by increasing either the applied potential or the inner radius. Power transmission efficiency increases with an increase in applied potential and a decrease in inner radius. Both these trends can be explained by changes in the electron/ion temperature or discharge volume. A gas heat transfer solver was implemented within PIC/MCC simulations and illustrated that heat transfer to the neutrals plays a integral part in determining discharge characteristics. The plasma-neutral collision frequency is the largest influencing factor for determining power transfer to the fluid. Different heating sources were also compared. This modeling shows that RF plasma discharge concept can potentially provide thrust in the milli-Newton range while meeting stringent power and size limitations and achieving specific impulse comparable to larger scale chemical propulsion systems.

Acknowledgments

The authors would like to thank Dr. J.P. Verboncoeur, Dr. C.K. Birdsall and the Berkeley Plasma Theory and Simulation Group for the use of their *XPDC1* code and providing assistance. We would also like to thank Dr. Mikhail Shneider for extremely valuable discussions of RF discharge physics. The computations reported in this paper were performed on 16 CPU Sunfire 4600 awarded through Sun Microsystems, Inc. Academic Excellence Grant #EDUD-7824-070336-US.

References

[1]Caceres, M., "The emerging nanosatellite market," *Aerospace America*, February 2001, pp. 16–18.

[2]Baker, A. and Underwood, C., "Micropropulsion from Snap to PALMSAT: When Does MEMS Become the Way Forward?" *Proceedings of NanoTech 2002 - "At the Edge of Revolution", AIAA-2002-5759, Houston, TX*, Sept. 2002.

[3]White, D., Schilling, J. H., Bushman, S., Spanjers, G., Bromaghim, D., Lake, J., and Dullingan, M., "AFRL MicroPPT Development for Small Spacecraft Propulsion," *33rd Plasmadynamics and Lasers Conference, AIAA 2002-2120, Maui, HW*, May 2002.

[4]Reed, G. D. and Hargus, W. A., "Complementary Plasma Density Measurements for the BHT-200-X3 Hall Thruster Plume," *42nd AIAA Joint Propulsion Conference, AIAA 2006-4992, Sacramento, CA*, July 2006.

[5]Maclay, T. and Tuttle, C., "Satellite Stationkeeping Of The ORBCOMM Constellation Via Active Control Of Atmospheric Drag: Operations, Constraints, And Performance," *Advances in the Astronautical Sciences, Part I*, Vol. 120, 2005, pp. 763–773.

[6]Ziemer, J., Gamero-Casta, M., Hruby, V., Spence, D., Demmons, N., McCormick, R., Roy, T., Gasdaska, C., Young, J., and Connolly, B., "Colloid Micro-Newton Thruster Development for the ST7-DRS and LISA Missions," *41st AIAA Joint Propulsion Conference, AIAA-2005-4265, Tucson, Arizona*, July 2005.

[7]Alves, M., Lieberman, M., Vahedi, V., and Birdsall, C., "Sheath voltage ratio for asymmetric rf discharge," *Journal of Applied Physics*, Vol. 69, No. 7, 1991.

[8]Leiter, H. and Feili, D., "RIT 15S- A Radio Frequency Ion Engine for High Specific Impulse Operation," *37th AIAA Joint Propulsion Conference*, July 2001, AIAA-2001-3491.

[9]Pollard, J., Lichtin, D., and Cohen, R., "RF Discharge Electrothermal Propulsion: Results from a Lab-Scale Thruster," *23rd AIAA Joint Propulsion Conference*, 1987, AIAA-1987-2124.

[10]Groh, K. and H.W.Loeb, "State-of-the-Art of Radio Frequency Ion Thrusters," *Journal of Propulsion and Power*, Vol. 7, No. 4, 1991, pp. 573–579.

[11]Brewer, L., Karras, T., and Grahm, D., "Preliminary Results of a High Power RF Thruster Test," *25th AIAA Joint Propulsion Conference*, 1989, AIAA-1989-2382.

[12]Olson, L., "Operation of a 50 W Radio Frequency Plasma Thruster," *37th AIAA Joint Propulsion Conference*, 2001, AIAA-2001-3903.

[13]Olson, L., "A More Efficient Radio Frequency Plasma Thruster," *35th AIAA Joint Propulsion Conference*, 1999, AIAA-1999-2437.

[14]A, M. and Hushfar, F., "Radio Frequency Heating of a Dense Moving Plasma," *AIAA Electric Propulsion Conference*, March 1963, 63045-63.

[15]Raizer, Y., Shneider, M., and Yatsenko, N., *Radio Frequency Capacitive Discharges*, CRC Press, 1995.

[16]Lieberman, M. and Lichtenberg, A., *Principles of Plasma Discharges and Materials Processing, 2nd Edition*, John Wiley and Sons, 2005.

[17]Moravej, M., Yang, X., Nowling, G., Change, J., and Hicks, R., "Physics of high-pressure helium and argon radio-frequency plasmas," *Journal of Applied Physics*, Vol. 96, No. 12, 2004.

[18]Sommerer, T., Hitchon, W., and Lawler, J., "Electron Heating Mechanisms in Helium rf Glow Discharges: A Self-Consistent Kinetic Calculation," *Physical Review Letters*, Vol. 63, No. 21, 1989.

[19]Novikova, T., Kalache, B., and Bulkin, P., "Numerical modeling of capacitively coupled hydrogen plasmas: Effects of frequency and pressure," *Journal of Applied Physics*, Vol. 93, No. 6, 2003.

[20]Okhrimovskyy, A., Bogaerts, A., and Gijbeis, R., "Incorporating the gas flow in a numerical model of rf discharges in methane," *Journal of Applied Physics*, Vol. 96, No. 6, 2004.

[21]Moravej, M., Yang, X., and Hicks, R., "A radio-frequency nonequilibrium atmospheric pressure plasma operating with argon and oxygen," *Journal of Applied Physics*, Vol. 99, 2006.

[22]Yuan, X. and Raja, L., "Computational Study of Capacitively Coupled High-Pressure Glow Discharges in Helium," *IEEE Transactions on Plasma Science*, Vol. 31, No. 4, 2003.

[23]White, P. S., Best, S., Hrbud, I., Hartsfield, R., and Rose, M., "RF Plasma Thruster for SmallSat Applications," *35th AIAA Joint Propulsion Conference*, 1999, AIAA 1999-2438.

[24]White, P., *Preliminary Investigation of an RF Plasma Thruster*, Master's thesis, Auburn University, 1999.

[25]Stein, W., Alexeenko, A., and Hrbud, I., "Performance Modeling of an RF Coaxial Plasma Thruster," *43rd AIAA Joint Propulsion Conference*, 2007, AIAA 2007-5292.

[26]Hrbud, I., Kemp, G. E., Yan, A. H., and Gedrimas, J. G., "Review of RF Plasma Thruster Development," *IEPC Paper 2007-309, 30th International Electric Propulsion Conference, Florence, Italy.*, Sept. 2007.

[27]White, P., "Preliminary Investigation of an RF Plasma Thruster, MS Thesis, Auburn University," 1999.

[28]Birdsall, C., "Particle-in-Cell Charged-Particle Simulations Plus Monte Carlo Collisions With Neutral Atoms, PIC-MCC," *IEEE Transactions on Plasma Science*, Vol. 19, No. 2, april 1991.

[29]Lawler, J. and Kortshagen, U., "Self-consistent Monte Carlo simulations of the positive column of gas discharges," *Physics D: Applied Physics*, Vol. 32, 1999, pp. 3188–3198.

[30]*Cylindrical Plasma Device 1-D Bounded Electrostatic Code*, Plasma Theory and Simulation Group, University of California, Berkeley, 2001.

[31]Raizer, Y. P. and Shneider, M., "Coaxial Medium-Pressure RF Discharge: Dynamics of Plasma Oscillations," *Plasma Physics Reports*, Vol. 21, 1995, pp. 260–267.

[32]Ivanov, M., Markelov, G., and Gimelshein, S., "Statistical Simulation of Reactive Rarefied Flows: Numerical Approach and Applications," *7th Joint Thermophysics and Heat Transfer Conference*, 1998, AIAA 98-2669.

[33]Raizer, Y., *Gas Discharge Physics*, Springer-Verlag, 1991.